Are finite elements appropriate for use in molecular dynamic simulations?

Lutz Nasdala, Andreas Kempe, Raimund Rolfes

Institute of Structural Analysis, Leibniz Universität Hannover, 30167 Hannover, Germany

Abstract

The applicability of finite elements for molecular dynamic simulations depends on both the structure's dimensions and the underlying force field type. Shell and continuum elements describe molecular structures only in an average sense, which is why they are not subject of this paper. In contrast, truss and beam elements are potentially attractive candidates when it comes to accurately reproducing the atomic interactions. However, special considerations are required for force fields that use not only two-body, but also multi-body potentials. For the example of bending and torsion energies it is shown how standard beam element models have to be extended to be equivalent to classical molecular dynamic simulations.

Keywords: C. Modeling, C. Computational mechanics, C. Finite element analysis (FEA), A. Carbon nanotubes, C. MDFEM

1. Introduction

Originally developed to solve structural engineering problems, the finite element (FE) method has found its way into a variety of application areas. Nowadays even molecular dynamic (MD) simulations are performed using commercial FE programs. One may wonder if this makes sense, because the two methods are quite different:

- A FE analysis converges to the exact solution when the mesh is sufficiently fine. The number of bonds in MD simulations depends on the interatomic distances and is not subject to change.
- While finite elements usually make use of first or second order shape functions, bond energies can be of tenth or even twelfth order.

The fact that, nevertheless, FE codes are used for MD simulations, is mainly due to the following two reasons:

- FE software is widely used and very popular in structural engineering, quite easy to use and comes along with powerful pre- and post-processing options and efficient solvers. When regarding molecular structures as multi-body systems with atoms as point masses and bonds as springs, it provides a convenient tool for MD simulations as well.
- Due to their quite general applicability, FE codes can be used to couple continuum and atomistic simulations. For an overview of multiscale methods, the reader is referred to the work by Miller and Tadmor (2009) who compare fourteen different techniques.

This paper aims to show the challenges and pitfalls when using standard finite elements for MD simulations, especially with regard to the following problems:

- Multi-body potentials connect three or more atoms.
- Bond energies are independent of the atoms' rotational degrees of freedom.
- A distinction between natural and equilibrium bond lengths and angles is necessary. That is, unlike continuum structures, most molecular systems contain large amounts of potential energy even in an unloaded equilibrium state.

From a mechanical point of view, shell elements, even though widely used for the simulation of e. g. multi-walled carbon nanotubes, are not capable of describing atomic interactions exactly. Therefore shell elements as well as continuum elements which can be applied to simulate micro- and macrostructures are not discussed here. In addition to the obvious candidates which include trusses, beams and spring elements, we will introduce an extended beam model for small deformations as well as special user elements which can be used for large deformations. The different models are compared for the example of carbon nanotubes with and without Stone-Wales defects subjected to different kinds of loading.

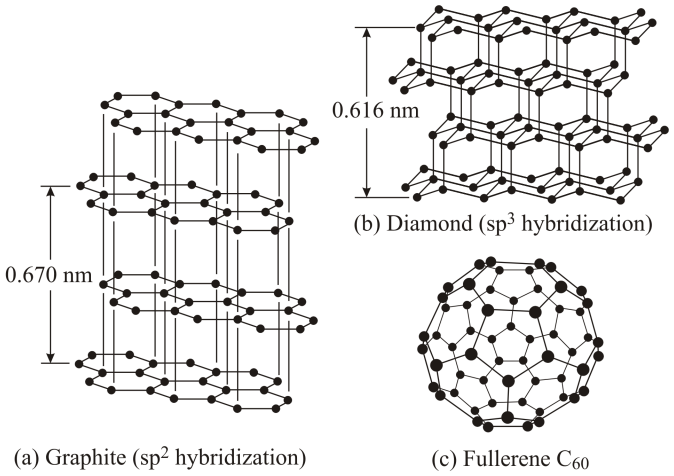

Figure 1: Modifications of elemental carbon

2. Force fields

2.1. Energy potentials

The possibilities and limits of particle molecular dynamics are closely related to the development of the computer. The first MD simulation was carried out by Alder and Wainwright (1957). They developed a model containing a few hundred particles that interact through elastic collisions with each other. In this way, they could simulate the phase transition from liquid to solid. Rahman (1964) were the first to use the Lennard-Jones potential in molecular dynamics in order to examine the properties of liquid argon.

Since then, various force field approaches have been developed to describe the different atomic interactions. From a mechanical point of view, a force field can be seen as data basis containing stiffnesses and strengths for chemical and physical bonds. The stiffnesses are neither constant nor dependent on only two atoms, but a function of the distances and angles of a whole bunch of atoms. Thus, some force fields can only be applied to very specific molecules.

Throughout this paper, we apply the general-purpose DREIDING force field developed by Mayo et al. (1990). Its functional form contains linear (harmonic) as well as nonlinear (anharmonic) potentials to account for small and large deformations. Thus it serves as an adequate example to study the approximation capabilities of different finite elements. As a so-called class I force field, is has been parameterized based on element type, hybridization and connectivity for many chemical elements. In the following, however, to keep things simple, we concentrate on sp^2 hybridized carbon.

As shown in Figure 1, sp^2 hybridized carbon atoms form graphite. The different layers, which are called graphene, consist of hexagons. They are connected to each other only by means of physical bonds, so-called van der Waals bondings. Carbon nanotubes which were discovered by Iijima (1991) can be seen as a special case of graphene. Note that the nanotubes' caps, like fullerenes, also contain pentagons. In diamond, carbon is sp^3 hybridized which allows for a fourth chemical bond.

2.2. Linear and nonlinear approaches

From a mechanical point of view, molecules like multi-body systems can be either statically determinate or indeterminate. In the latter case, the equilibrium state can usually only be given approximately and has to be determined within a so-called conformational analysis. To overcome numerical problems caused by highly nonlinear energy functions, it is good practice to start with a linear approach.

In Figure 2, linear and nonlinear energy potentials of the DREIDING force field and the corresponding stiffnesses are compared for the example of sp^2 hybridized carbon. The equilibrium distance or, to be more precise, the natural bond distance is given to $R_\mathrm{e} = 1.42\,\text{Å}$. Bond stretch interactions are described either by a simple harmonic oscillator $E_\mathrm{B}^\mathrm{lin}$ resulting in a constant bond stiffness $c_\mathrm{B}^\mathrm{lin}$ or

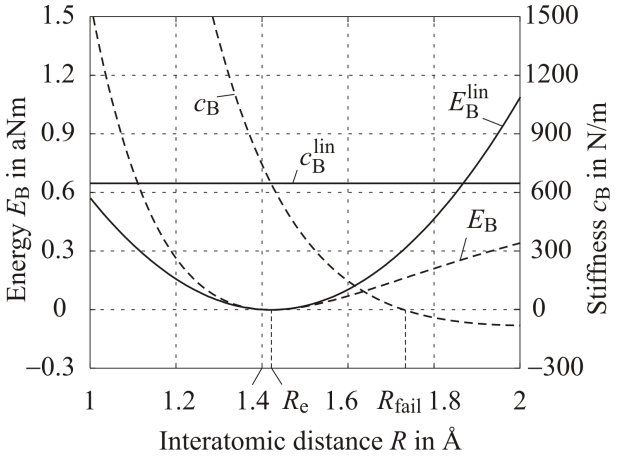

(a) Bond stretch: linear/nonlinear stiffness and energy

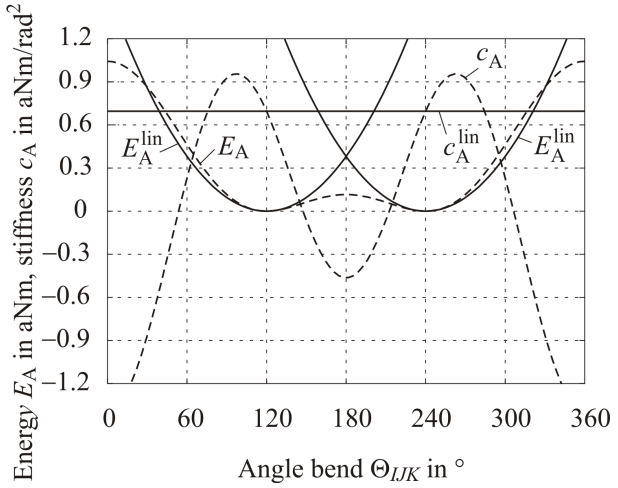

(b) Bending: linear/nonlinear stiffness and energy

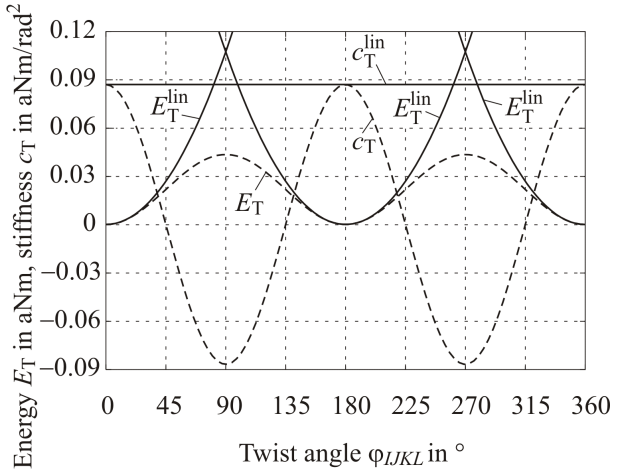

(c) Torsion: linear/nonlinear stiffness and energy

Figure 2: Energy potentials for sp^2 hybridized carbon according to DREIDING force field

an exponential Morse function E_B that allows to account for bond breaking. Note that the corresponding bond stiffness c_B decays with increasing interatomic distance and becomes negative when the limit distance $R_{fail} = 1.73$ Å is exceeded. Bending and torsion are either modeled using harmonic angle potentials E_A^{lin} and E_T^{lin} with constant spring stiffnesses c_A^{lin} and c_T^{lin} or by harmonic cosine potentials E_A/E_T and nonlinear stiffnesses c_A/c_T, respectively. Due to their sp^2 hybridization, carbon atoms C_2 or rather C_R (aromatic ring) have two natural bend angles, $\Theta_J^0 = 120°$ and 240°, and two natural twist angles, $\varphi_{JK}^0 = 0°$ and 180°. For $\Theta_{IJK} = 180°$ or rather $\varphi_{IJKL} = 90°$ and 270°, the nonlinear approaches for bending/torsion have a slope equal to zero and enable a transition between the natural angles. Note that a torsional loading also affects the deformation of neighboring bonds as shown in Figures 3 and 4 for both natural angles.

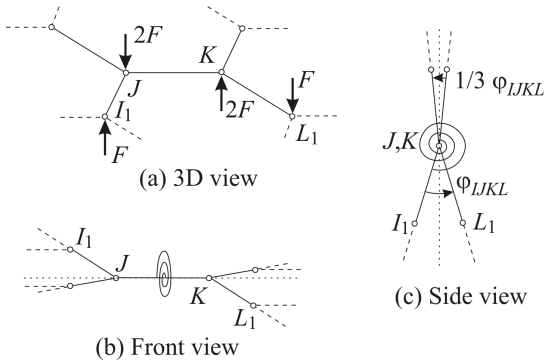

Figure 3: Torque of atoms with natural twist angle $\varphi_{JK}^0 = 0°$

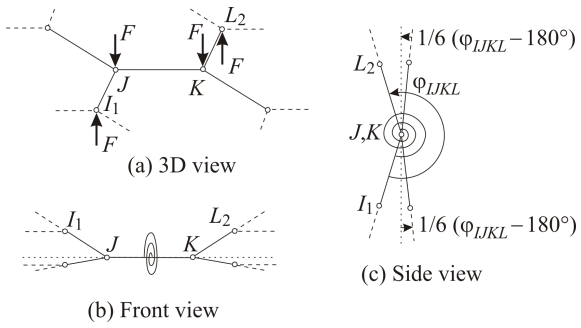

Figure 4: Torque of atoms with natural twist angle $\varphi_{JK}^0 = 180°$

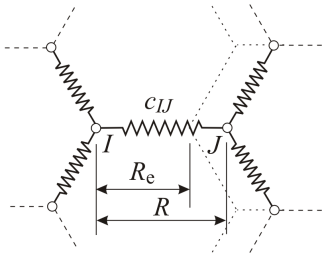

Figure 5: Modeling of bond stretch using spring elements

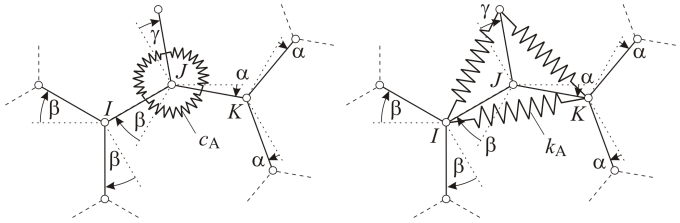

(a) Rotational spring enrichment (force field approach) (b) Normal spring enrichment

Figure 6: Different truss element models for angle bend

3. FE models using standard elements

The modeling of bond stretch is very straightforward. As shown in Figure 5, a spring, which is the simplest finite element, would suffice. Of course, truss and beam elements can be used as well. Unfortunately, all these elements have only two nodes, so that a direct modeling of multi-body potentials is impossible.

3.1. Truss element models

At first glance, it seems obvious to use a truss model since truss nodes, like atoms, have only translational degrees of freedom. However, it requires some extra effort to consider bending, and modeling of torsion is not even possible.

Truss models have to be enriched by either rotational or normal springs. Rotational springs require the introduction of truss angles as additional degrees of freedom, defined and constrained by the nodal coordinates. Normal springs have the disadvantage that the bending potential can only be represented by a complex geometric relationship if deformations become large.

For the example molecule given in Figure 6, the bond angle Θ_{IJK} is defined by the coordinates of the truss nodes I, J and K. Since the structure is statically determinate, all bonds on the left will rotate by the same angle β as bond IJ, and all bonds on the right will rotate by the same angle α as bond JK. The deformation of both models is equivalent with the reference solution given by the force field method.

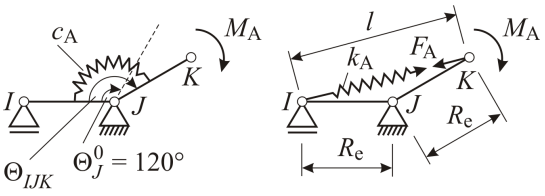

Figure 7: Conversion of rotational spring to normal spring

To demonstrate the duality of rotational and normal spring enrichment, without loss of generality, we assume that bonds IJ and JK are both of length R_e and use a natural angle of $\Theta_J^0 = 120°$. As shown in Figure 7, node K is subjected to a bending moment

$$M_A = \int_{\Theta_J^0}^{\Theta_{IJK}} c_A(\tilde{\Theta}_{IJK})\, d\tilde{\Theta}_{IJK} \tag{1}$$

where the nonlinear bending stiffness c_A is known. The force

$$F_A = \int_{l_0}^{l} k_A(\tilde{l})\, d\tilde{l} \tag{2}$$

depends on the normal spring's current and initial length

$$\begin{aligned} l &= 2R_e \sin\left(\frac{\Theta_{IJK}}{2}\right) \\ l_0 &= l(\Theta_{IJK} = \Theta_J^0) = \sqrt{3}R_e \quad . \end{aligned} \tag{3}$$

The equilibrium of forces directly yields the force

$$F_A = \frac{M_A}{R_e \cos\left(\frac{\Theta_{IJK}}{2}\right)} \tag{4}$$

as a function of the moment $M_A = M_A(\Theta_{IJK})$ and the current angle Θ_{IJK}. By deriving F_A with respect to l, we get the nonlinear normal spring stiffness as

$$k_A = \frac{dF_A}{dl} = \frac{dF_A}{d\Theta_{IJK}} \frac{d\Theta_{IJK}}{dl} \quad . \tag{5}$$

While the derivative $\frac{dF_A}{d\Theta_{IJK}}$ depends on the chosen approach for the bending energy, the derivative $\frac{d\Theta_{IJK}}{dl}$ can be formed solely from geometric considerations.

Since standard finite elements can consider only a constant stiffness $c_{\mathrm{A}}^{\mathrm{lin}} = K_{IJK}$, we now assume that deformations are small: $\Theta_{IJK} \to \Theta_J^0$. Then, moment

$$M_{\mathrm{A}}^{\mathrm{lin}} = K_{IJK}[\Theta_{IJK} - \Theta_J^0] \tag{6}$$

and force

$$F_{\mathrm{A}}^{\mathrm{lin}} = k_{\mathrm{A}}^{\mathrm{lin}}(l - l_0) \tag{7}$$

depend linearly on the angle Θ_{IJK} or rather the length l. The normal stiffness

$$k_{\mathrm{A}}^{\mathrm{lin}} = \frac{4K_{IJK}}{R_{\mathrm{e}}^2} \quad . \tag{8}$$

is proportional to the bending stiffness K_{IJK}.

As already mentioned, truss models cannot handle torsion potentials. Hence, they are limited to planar structures such as graphene, see e. g. the models developed by Wang (2004), Leung et al. (2005), Zhang et al. (2007) and Zhu and Wang (2007), or selected spatial structures. For instance, Odegard et al. (2002) and Nahas and Abd-Rabou (2010) use the truss model shown in Figure 6(b) for the simulation of defect-free carbon nanotubes subjected to uniaxial loading.

Lacking torsional stiffness, truss models are quite instable. Simulations performed by the authors demonstrate that nanotubes with Stone-Wales defects lead to convergence problems due to rigid body motions. Even for defect-free nanotubes, numerical robustness cannot be guaranteed. In case of a bending load, for example, there is no resistance against the inversion of individual atoms. In contrast to bending shells, the structural behavior is comparable to that of a membrane shell where the lack of bending stiffness leads to unrealistic local snap-through problems of one or more atoms.

Comparing truss and beam models, Hu et al. (2005) come to the conclusion that truss models cannot describe carbon nanotubes since the Poisson's ratio ν would have to be set to a constant value of $1/3$ which is not correct.

3.2. Beam element models

A very straightforward beam model which was proposed by Li and Chou (2003b) is to link the beam elements by means of rigid connections as shown in Figure 8(a). Since the modeling effort is low, we denote this approach "standard beam model".

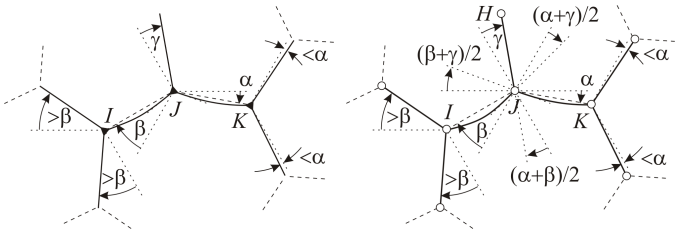

(a) With rigid corners (b) With joints and constraints

Figure 8: Different beam element models for angle bend

An alternative way is to connect the beams with the help of hinges (2D) or joints (3D) and to constrain the rotational degrees of freedom. For the example depicted in Figure 8(b), the rotation of node J of bond JK is given as $\frac{\beta+\gamma}{2}$ with β and γ denoting the rotation of bonds IJ and HJ, respectively. The other beam nodes are constrained in an analogous way. Note that the bond angles have to be determined from the nodal coordinates. This approach has the advantage over the standard beam model that only translational degrees of freedom remain.

Several variants of the standard beam model can be found in the literature. For example, Wang and Wang (2004) examine the failure mechanism of multi-walled carbon nanotubes using the commercial FE code Abaqus with beam element B33, a 3D Euler Bernoulli beam. Under bending loading, local buckles occur that are formed like ribs. This phenomenon can also be observed in experiments. To consider the Morse potential, Chwal (2011) replaces the constant normal stiffness of the B33 element with a corresponding user material model. The Abaqus beam element B31H, which adopts a hybrid Timoshenko formulation, is used by Saavedra Flores et al. (2011). The nonlinear bond stretch behavior is imposed by an Ogden hyperelastic material law. Chen and Cao (2006) and Ding et al. (2007) use the quadratic Timoshenko beam element B32.

Further examples include Tserpes and Papanikos (2005), Sakhaee-Pour and Ahmadian (2007), Fan et al. (2009) and Shokrieh and Rafiee (2010) which use the Euler Bernoulli element BEAM4 of the commercial software Ansys.

How problematic the application of beam elements for nanostructures is can be deduced from the findings of Yoon et al. (2004). They come to the conclusion that Timoshenko beam elements should be preferred over Euler-Bernoulli beams when calculating the wave propagation speed within carbon nanotubes.

? address "Yakobson's paradox" concerning the large scatter of the elastic modulus of SWCNT obtained in atomistic and continuum approximations. In order to determine equivalent thickness and Poisson's ratio for C-C bonds uniquely, they assume isotropic material behavior and equivalence between bending potential and bending stiffness of the shear-flexible Timoshenko beam.

The issue is not whether bonds possess a transversal shear stiffness or not, but if it is possible to identify beam constants at all. While the nonlinear normal stiffness EA can be derived directly from the bond stretch energy E_A, it is not trivial to determine bending and torsional stiffness.

As demonstrated in the following, an unambiguous identification of the beam's bending stiffness EI is only possible for planar structures, i. e., when torsion can be neglected. For demonstration purposes, we consider a tension test and a shear test of graphene. The unit cells are depicted in Figures 9 and 10. Without loss of generality, we assume small deformations and neglect bond length changes: $R = R_\mathrm{e}$ for $EA = R_\mathrm{e} c_\mathrm{B} \to \infty$. The total energies of the force field approach

$$\begin{aligned} W_\mathrm{tension} &= 4\frac{1}{2}c_\mathrm{A}\Psi^2 + 2\frac{1}{2}c_\mathrm{A}(2\Psi)^2 = 6c_\mathrm{A}\Psi^2 \\ W_\mathrm{shear} &= 4\frac{1}{2}c_\mathrm{A}\Psi^2 = 2c_\mathrm{A}\Psi^2 \end{aligned} \tag{9}$$

can be given as a function of the truss angle Ψ. Also shown in Figures 9 and 10 are the deformations and bending moment curves of the standard beam element model. According to the direct displacement method and considering the nodal angle $\varphi = \frac{\Psi}{3}$, we get

$$\begin{aligned} M_\mathrm{tension} &= 6\frac{EI}{R_\mathrm{e}}\Psi \\ M_\mathrm{shear} &= 2\frac{EI}{R_\mathrm{e}}\Psi \end{aligned} \tag{10}$$

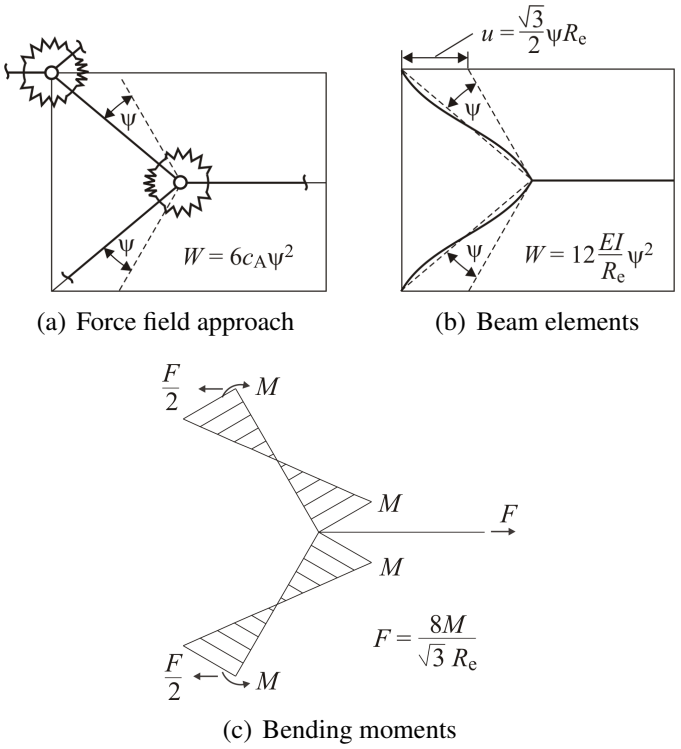

(a) Force field approach (b) Beam elements

(c) Bending moments

Figure 9: Unit cell of graphene: tension test

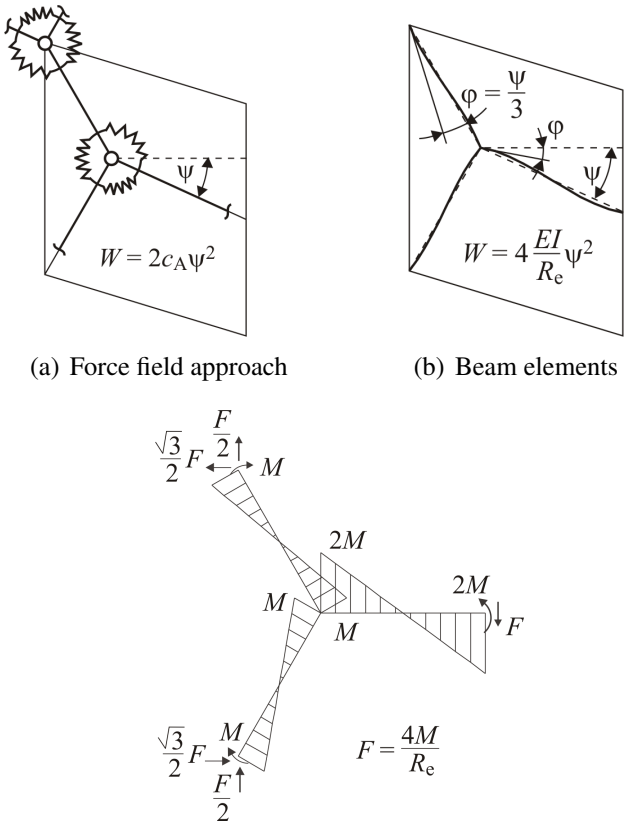

(a) Force field approach (b) Beam elements

(c) Bending moments

Figure 10: Unit cell of graphene: shear test

as the corresponding moments and

$$W_{\text{tension}} = \frac{1}{2}Fu = 12\frac{EI}{R_e}\Psi^2$$
$$W_{\text{shear}} = \frac{1}{2}FR_e\Psi + 2\frac{1}{2}M\varphi - \frac{1}{2}(2M)\varphi = 4\frac{EI}{R_e}\Psi^2 \tag{11}$$

as the total energies. Equating the energies from Eqs. (9) and (11) leads to the bending stiffness

$$EI = \frac{1}{2}R_e c_A \tag{12}$$

for the "standard beam model" (SBM).

Nevertheless, though the bending stiffness is identical for both load cases, a calculation of the bending test as depicted in Figure 6 leads to incorrect results. As shown in Figure 8(a), due to the beam curvature, the bonds on the left next to bond IJ are rotated by an angle larger than β whereas the bonds on the right next to bond JK are rotated by an angle smaller than α. Note that the result from the alternative beam model shown in Figure 8(b) is equally bad.

As if this was not enough, in case of spatial nanostructures, even the parameter identification is ambiguous. To take into account that torque of beams weakens the overall stiffness, the bending stiffness is increased by many authors. As proposed by Li and Chou (2003a, 2004), e. g. Lau et al. (2004), Kalamkarov et al. (2006) and Fan et al. (2009) use a bending stiffness of

$$EI = R_e c_A \tag{13}$$

which is twice as much as the analytical solution from Eq. (12). Normal and torsional stiffness are given as $EA = R_e c_B$ and $GJ = R_e c_T$, respectively.

Another suggestion was made by Hu et al. (2005, 2007) who derive a bending stiffness of

$$EI = \frac{c_B R_e^3 (c_B R_e^2 + 3c_A)}{36(c_B R_e^2 - c_A)} \quad . \tag{14}$$

Using the Dreiding parameters given in Figures 2(a) and 2(b), $R_e = 1.42\,\text{Å}$, $c_B^{\text{lin}} = 648.6\,\text{N/m}$ and $c_A^{\text{lin}} = 0.6952\,\text{aNm/rad}^2$, yields $EI = 6.318 \cdot 10^{-29}\,\text{Nm}^2$ which lies in between the analytical solution $EI = 4.936 \cdot 10^{-29}\,\text{Nm}^2$ and the bending stiffness $EI = 9.872 \cdot 10^{-29}\,\text{Nm}^2$ from the approach by Li and Chou (2003a, 2004). The torsional stiffness derived by Hu et al. (2005, 2007), $GJ = 2R_e c_T = 2.468 \cdot 10^{-29}\,\text{Nm}^2$ with $c_T^{\text{lin}} = 0.08690\,\text{aNm/rad}^2$ from Figure 2(c), is twice as much as the value given by Li and Chou (2003a, 2004). As expected, the normal stiffness is set to $EA = R_e c_B$.

Many other approaches are possible. For instance, assuming a circular beam cross-section and a Poisson's ratio $\nu = 0$, we propose a torsional stiffness of $GJ = \frac{E}{2(1+\nu)}2I = EI$ when using the analytical bending stiffness from Eq. (12).

For completeness, it should be mentioned that the standard beam approach is also not capable of simulating the torsion test shown in Figures 3 and 4. It is not possible to decouple bending and torsion since the twist angle φ_{IJKL}, which is the angle between the two planes IJK and JKL, can be created both by a twist of beam JK and by bending of the beams IJ and KL. Further, as already discussed for the example of the bending test, the curvature of the beam leads to false bond rotations.

To conclude this section, we would advise against using the presented standard element FE models. Of course it is possible to adapt the standard beam model to obtain acceptable approximations for specific applications, but when trying to reproduce force fields as precisely as possible, node-by-node coupling of rotational degrees of freedom should be avoided. Exceptions include two-dimensional models such as the polymer network simulated by Wang et al. (2003) since torsion can be neglected in this case.

4. Extended beam element models

The idea behind the extended beam element models is to decouple the different energy types by means of the superposition technique shown in Figures 11 and 12. Special 3-node and 4-node elements are needed to handle bending and torsion separately. Depending on the application, these macro elements may either be composed of standard beam elements or implemented as user finite elements. Rotational degrees of freedom are allowed internally, but must be eliminated on the element level. Consequently,

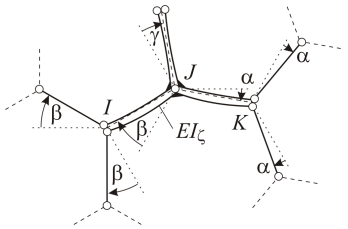

Figure 11: Extended beam element model for angle bend

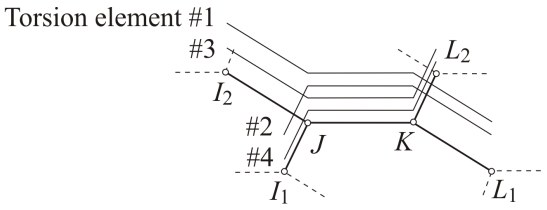

(a) Superposition technique: 4 torsion elements for bond JK

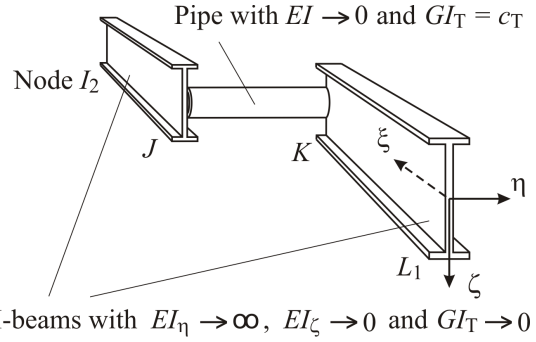

(b) Torsion element #1, composed of standard beam elements

Figure 12: Extended beam element model for torsion

all macro elements are to be connected by means of joints.

For instance, Parvaneh et al. (2009) use nonlinear springs and connector elements provided by Abaqus as base elements. Similar to torsional springs applied by e. g. Meo and Rossi (2006) and Rossi and Meo (2009), connector elements make use of relative rotation between two nodes while the global rotations are ignored.

A special case of the extended beam model are user elements based on potentials of Tersoff-Brenner type because a large number of atomic interactions has to be considered, see Brenner (1990) for details. For example, Theodosiou and Saravanos (2007, 2011) developed a 6-node "benzene element" based on these potentials. The AFEM element proposed by Liu et al. (2004) consists of 10 carbon atoms and Wackerfuß (2009) even created a special 22-node finite element.

The mesh generation costs of the overlay technique are quite high compared to the standard beam element model when using separate bond stretch, bending and torsion elements. For instance, each angle Θ_{IJK} requires its own bending element so that for graphene a total of four bending elements include bond IJ. Moreover, bond IJ also belongs to a total of twelve torsion elements: four times as middle segment and eight times as end segment. However, the total number of degrees of freedom is only half as large because only translational degrees of freedom are needed and the parameter identification has a unique solution.

4.1. Small deformations

As shown in Figure 11, two beam elements that are welded together function as rotational spring. In accordance with the reference solution presented in Figure 6(a), all bonds on the left rotate exactly by β while the bonds on the right rotate by α.

The superposition technique also makes it possible to match the reference solution for torsion given in Figures 3 and 4 exactly. The 2-node bond stretch elements, the 3-node bending elements from Figure 11 and the 4-node torsion elements from Figure 12 are connected by only using their translational degrees of freedom. Figures 13(a) and 14(a) show all elements that are superposed for the natural angles $\varphi^0_{JK} = 0°$ and 180°.

In order to decouple bending and torsion within the torsion element, the engineering constants of pipe and I-beams have to be chosen such that only the pipe element, which acts as a coil spring, possesses strain energy, see Figure 12(b). Torsional loadings like the ones given in Figures 13(b) and 14(b) not only lead to torque (Figures 13(d) and 14(d)) but also to bending moments (Figures 13(c) and 14(c)). The resulting bending energy vanishes when the bending stiffnesses are chosen to go to zero or rather infinity. Then the torsional energy E_T is produced exclusively by the pipe element. For demonstration purposes, let us assume that deformations are small which leads a

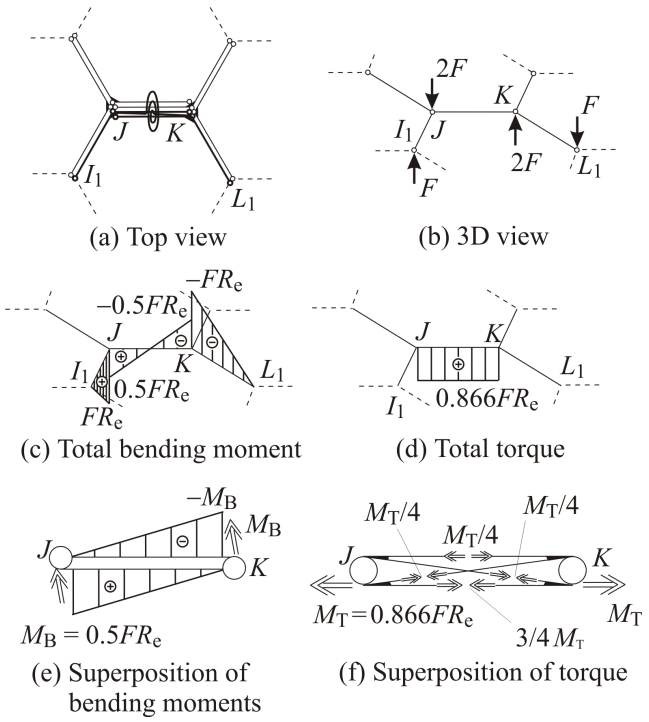

(a) Top view (b) 3D view

(c) Total bending moment (d) Total torque

(e) Superposition of bending moments (f) Superposition of torque

Figure 13: Internal beam forces for natural angle $\varphi^0_{JK} = 0°$

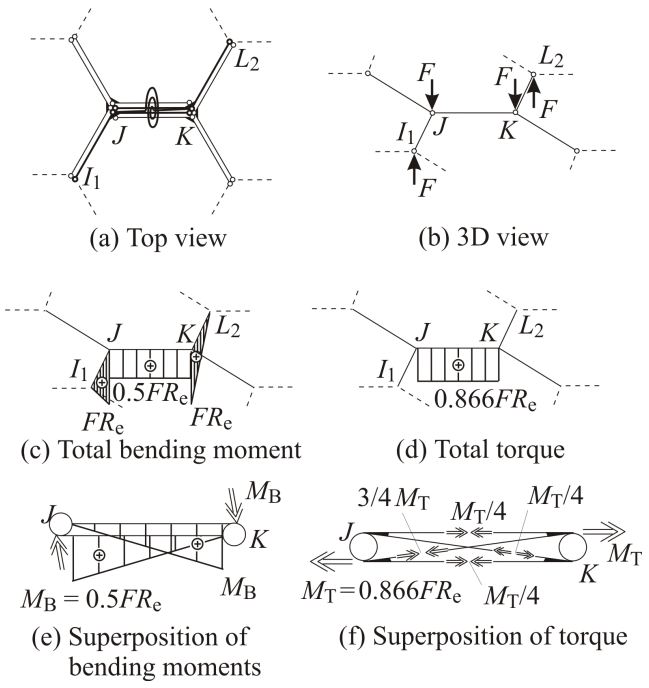

(a) Top view (b) 3D view

(c) Total bending moment (d) Total torque

(e) Superposition of bending moments (f) Superposition of torque

Figure 14: Internal beam forces for natural angle $\varphi^0_{JK} = 180°$

torsion energy of

$$\begin{aligned} E_{\mathrm{T}}^{\mathrm{lin}} &= \lim_{EI_\eta \to \infty} \int -\frac{1}{2} M_{\mathrm{B}} w'' \, d\xi \quad + \int_{\xi_J}^{\xi_K} \frac{1}{2} M_{\mathrm{T}} \varphi' \, d\xi \\ &= \lim_{EI_\eta \to \infty} \int \frac{1}{2} \frac{M_{\mathrm{B}}^2}{EI_\eta} \, d\xi \quad + \int_{\xi_J}^{\xi_K} \frac{1}{2} \frac{M_{\mathrm{T}}^2}{GI_{\mathrm{T}}} \, d\xi \\ &= 0 \quad + \int_0^{R_{\mathrm{e}}} \frac{1}{2} \frac{M_{\mathrm{T}}^2}{c_{\mathrm{T}}^{\mathrm{lin}} R_{\mathrm{e}}} \, d\xi \end{aligned} \tag{15}$$

with $\{\ldots\}' = \frac{d\{\ldots\}}{d\xi}$.

As shown in the Figures 13(e) and 14(e), the bending moment is distributed between two bending elements: either I_1JK and JKL_1 or I_1JK and JKL_2. The indices "1" and "2" of nodes I and L denote the equilibrium state: cis-configuration (0°-element) for identical indices, trans-configuration (180°-element) in case of different indices.

Torque is distributed between four torsion elements: the two 0°-elements I_1JKL_1 and I_2JKL_2 and the two 180°-elements I_1JKL_2 and I_2JKL_1, as shown in Figures 13(f) und 14(f):

$$M_{\mathrm{T}}^{\mathrm{cis}} = \frac{3M_{\mathrm{T},I_1JKL_1}}{4} + \frac{M_{\mathrm{T},I_1JKL_2}}{4} + \frac{M_{\mathrm{T},I_2JKL_1}}{4} - \frac{M_{\mathrm{T},I_2JKL_2}}{4} \tag{16}$$

for the cis-configuration and

$$M_{\mathrm{T}}^{\mathrm{trans}} = \frac{M_{\mathrm{T},I_1JKL_1}}{4} + \frac{3M_{\mathrm{T},I_1JKL_2}}{4} - \frac{M_{\mathrm{T},I_2JKL_1}}{4} + \frac{M_{\mathrm{T},I_2JKL_2}}{4} \tag{17}$$

for the trans-configuration. The resulting twist angles are identical to the reference solution given in Figures 3(c) and 4(c).

4.2. Large deformations

Truss and beam elements normally have constant engineering parameters. They cannot be used as base elements for the 3- and 4-node bending and torsion elements if deformations become large. Apart from the question of how to describe nonlinear force field potentials, geometric nonlinearities complicate their application. For instance, at large tensile strains, even with linear elastic material, the force-deflection curve drops due to a reduction of the cross-section area. A workaround is to set the Poisson's ratio to zero. A better choice, however, is to use spring elements which do not have a cross-section area. Most

FE programs provide spring elements or rather connector elements where an arbitrary nonlinear force-deflection characteristic can be defined.

As already noted, the application of rotational springs requires the definition of bond angles as rotational degrees of freedom from the nodal coordinates. In order to reduce this modeling effort and to eliminate the rotational degrees of freedom on the element level, we have implemented bond stretch, bending and torsion elements as user-defined elements within the framework of the molecular dynamic finite element method (MDFEM), see Nasdala et al. (2010) for more details. Besides the aforementioned advantages of the extended beam model over the standard beam model, the MDFEM elements are characterized by the following beneficial features:

- There is no need to introduce initial strains or stresses because the natural distance R_e as well as the natural angles Θ_j^0 and φ_{JK}^0 are intrinsic element parameters. As a result, nodal coordinates only have to be given approximatively since the FE model automatically relaxes to the equilibrium state.

- A parameter identification procedure is obsolete since all parameters can be taken directly from the force field.

- Optionally, they are applicable to a small strain analysis using harmonic potentials, e. g. when the initial configuration is improved during a linear relaxation step.

There is no approximation of any kind, even in case of large deformations, i. e., the results are identical to a molecular dynamic simulation using any nonlinear force field potential.

5. Finite element analysis of carbon nanotubes

In the following, various simulations of carbon nanotubes are presented. The goal is to demonstrate the differences between the standard beam model and the extended beam model and to show the robustness of the MDFEM elements.

The mechanical and electrical properties of nanotubes depend on the chiral angle θ. Figure 15 shows

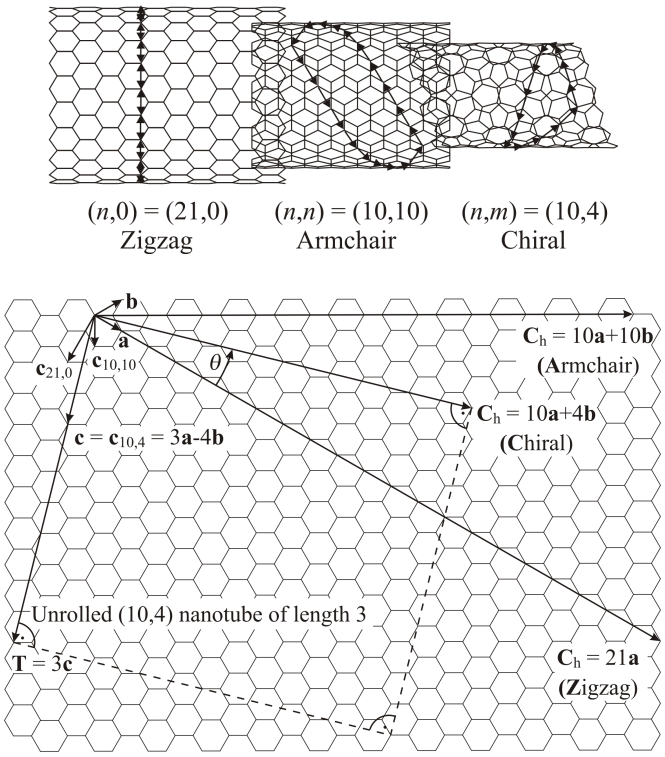

Figure 15: Classification of carbon nanotubes according to the chiral vector $\mathbf{C}_\mathrm{h} = n\mathbf{a} + m\mathbf{b}$

that the corresponding chiral vector $\mathbf{C}_\mathrm{h} = n\mathbf{a} + m\mathbf{b}$ can be expressed as a function of the base vectors $\mathbf{a}$ and $\mathbf{b}$ with the integer coefficients n and $m \in [0, n]$. Of particular interest are zigzag nanotubes $(n, 0)$ and armchair nanotubes (n, n).

5.1. Local tension tests

As a first example, we choose a (17,0) zigzag nanotube subjected to tensile loading. Figure 16 depicts three different load cases that have been examined. Load case 1 represents more or less a global tension test. For load cases 2 and 3, the nodal forces $F = 10^{-10}\,\mathrm{N}$ are applied locally.

The exact results of the extended beam model are obtained using MDFEM. They are compared to three variants of the standard beam model, i. e. to the three parameter sets for the bending and torsional stiffnesses given in section 3.2.

For comparison purposes, the deformations are assumed to be small and the equilibrium state established within the MDFEM conformational analysis is used as initial configuration also for the beam element models. The beams are modeled using Abaqus B33 elements based on Euler-Bernoulli beam theory.

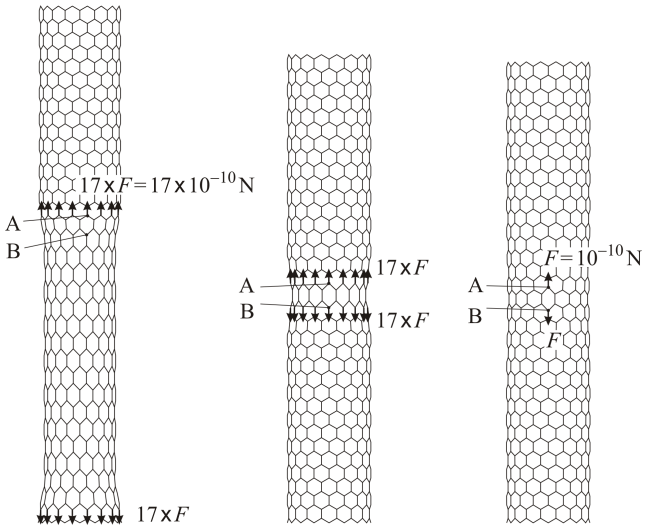

(a) Load case 1 (b) Load case 2 (c) Load case 3

		Load case 1	Load case 2	Load case 3
MDFEM	Δu in pm	0.5403	0.5273	0.3818
SBM/ Eq. (12)	Δu in pm	0.5442	0.5303	0.4471
	E_{rel} in %	0.72	0.57	17.10
Hu et al./ Eq. (14)	Δu in pm	0.4717	0.4629	0.3815
	E_{rel} in %	12.70	12.21	0.08
Li and Chou/ Eq. (13)	Δu in pm	0.3755	0.3730	0.2917
	E_{rel} in %	30.50	29.26	23.60

Figure 16: Local tension tests of (17,0) zigzag nanotube

Figure 16 shows the results of a static analysis with a deformation scale factor of 200. Moreover, the relative motion $\Delta u = u_B - u_A$ between nodes A and B including the relative errors with respect to the reference MDFEM solution are listed.

With relative errors of 0.72 % and 0.57 % for the axisymmetric load cases 1 and 2, a good agreement can be observed for the SBM parameter set. The high error of 17.10 % in load case 3 can be explained by the different local bend angles.

Hu et al. (2005, 2007) make use of a hexagonal unit cell as part of a graphene layer to identify the relation between the force field and beam stiffnesses. As a result, load case 3 shows only a small error of 0.08 %. However, load cases 1 and 2 differ from the reference solution by 12.70 % and 12.21 % , respectively. With an average error of about 28 %, the parameter set based on the approach by Li and Chou (2003a, 2004) yields a too stiff behavior for all load cases.

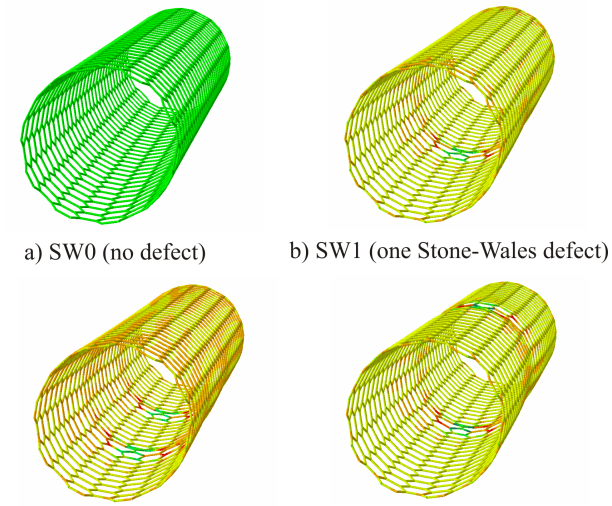

a) SW0 (no defect) b) SW1 (one Stone-Wales defect)

c) SW2 (two neighboring Stone-Wales defects) d) SW3 (two opposing Stone-Wales defects)

Figure 17: Equilibrium configurations of (10,10) armchair nanotubes

The example illustrates that standard beam models can be adapted to capture specific loading scenarios. A simulation of all load cases, however, is not possible. As a consequence, beam elements as well as truss elements should be avoided in favor of more precise models such as the extended beam model.

5.2. Global tension tests

In our next examples, we consider (10,10) armchair nanotubes with and without Stone-Wales defects subjected to large deformations, such that geometric as well as material failure can be observed. In FE analyses, different solution techniques can be applied to determine the structural response. For instance, in case of snap-through problems, a path-tracking algorithm such as Riks' method can be very useful. The goal is to demonstrate that MDFEM elements are applicable to different kinds of procedures such as a static analysis using the Riks arc-length method or the Euler backward and Hilber-Hughes-Taylor (HHT) implicit time integration schemes.

As in molecular dynamics, the first step of an MDFEM calculation is a conformational analysis. Figure 17 shows the obtained equilibrium configurations for a defect-free nanotube SW0 and three examples

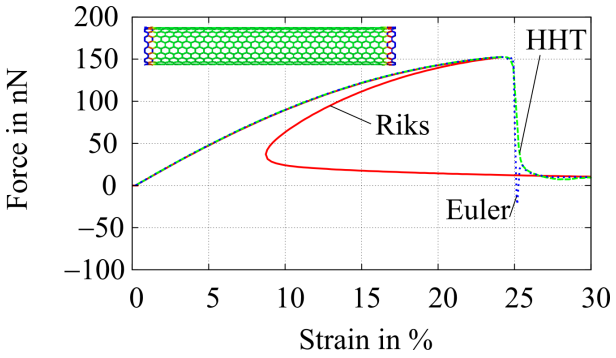

(a) defect group SW0

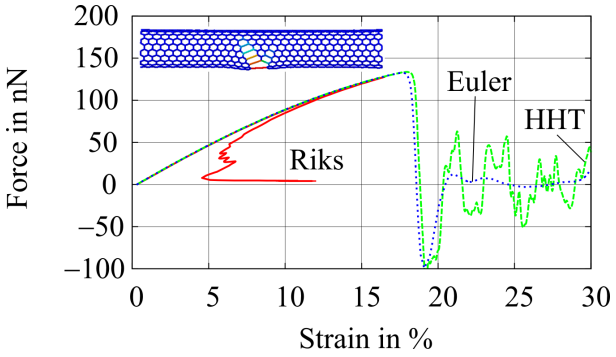

(b) defect group SW1

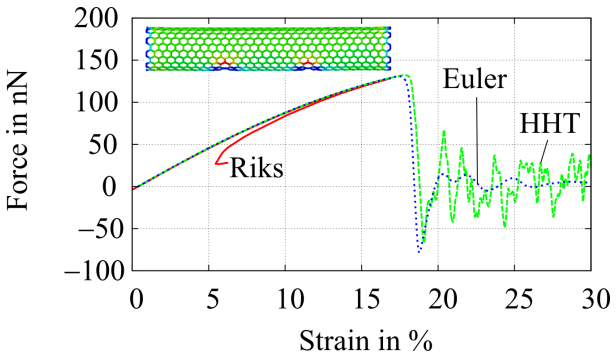

(c) defect group SW2

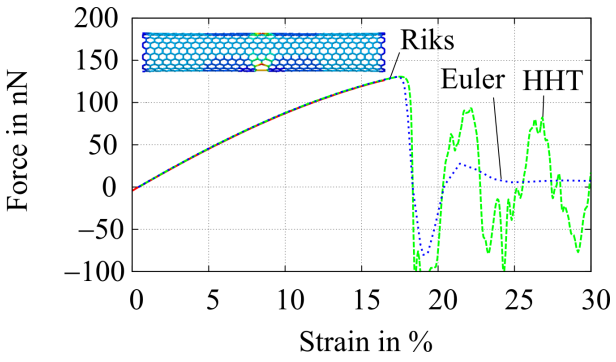

(d) defect group SW3

Figure 18: Comparison of FE solution techniques for tension test of carbon nanotubes with defects

with Stone-Wales defects at different locations labeled SW1, SW2 and SW3. The color coding shows the logarithmic strains of the individual bonds. It illustrates the deviation from the initial defect-free structure (green), which reaches its maximum in the vicinity of the defects (red).

When subjected to tension as depicted in load-deflection curves in Figure 18, the nanotubes fail due to bond breakage. Note that the pre-failure paths as well as the failure loads are identical for all three procedures. As bond failure is a dynamic process, the equilibrium path of the static Riks method differs from the two dynamic procedures. After failure, HHT and Euler backward solutions exhibit a dynamic equilibrium. The Euler backward method adopts large amounts of numerical damping, which is why the amplitudes are significantly smaller than the ones obtained using HHT. The snap-back-like behavior observed for the Riks method should not be confused with a stability problem. The nonlinearity of the load-deflection curve is caused by material failure.

An interesting result is that the failure load is reduced from 152 nN to about 130 nN no matter where the defects are located. The failure strain is also reduced from 25 % to 18 %. In the upper left corner of each load-deflection curve in Figure 18, the logarithmic bond strains are depicted at the onset of damage. While for the examples SW1, SW2 and SW3 bond breakage is induced by the defects, the defect-free tube SW0 starts to fail from the ends.

5.3. Bending, torsion and compression tests

A stability problem occurs, when the (10,10) armchair nanotubes are subjected to compression, torsion or bending. Again, we applied the three solution techniques but for reasons of clarity, Figure 19 only gives the load-deflection curves obtained with the static Riks method, as it is supposed to be the most efficient method when geometric failure such as snap through occurs.

The compression test reveals that carbon nanotubes are imperfection sensitive since defects (SW1, SW2, SW3) lead to an enormous drop of the load-deflection curve. Another important result is that the Riks method is not applicable to defect-free nanotubes: Due to the perfect symmetry, the Riks

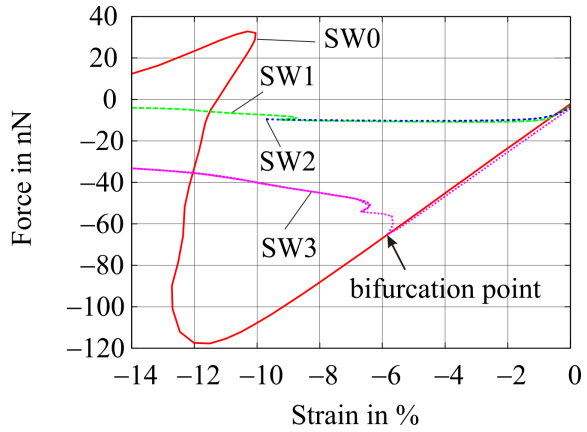

(a) Compression

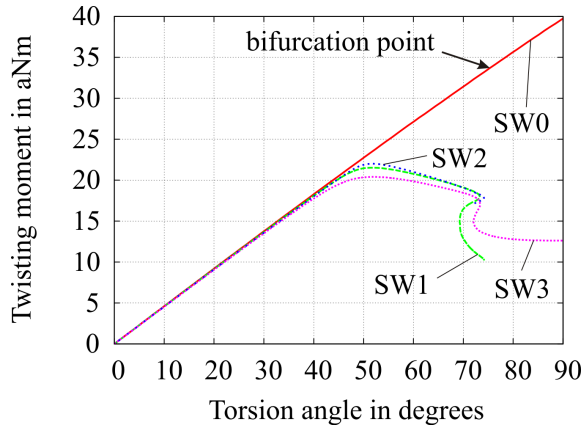

(b) Torsion

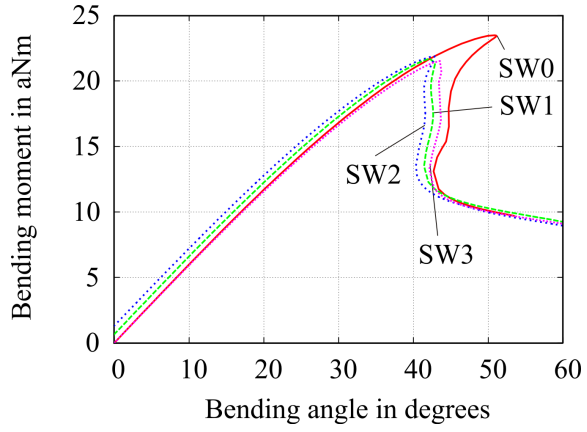

(c) Bending

Figure 19: Stability problems simulated using the Riks arc-length method

method fails to branch at the bifurcation point. The critical load for SW0 is not 120 nN, but 65 nN as both dynamic simulations, which are not presented here, show. While the critical load for SW1 und SW2 is 10 nN, the critical load of SW3 decreases only little, namely to 62 nN. This effect can be explained by the symmetry of the defects SW3 which are located at opposite sides in the center of the tube, cf. Figure 17.

The torsion test is another good example for the fact that defects serve as imperfections and thus turn a bifurcation problem into a snap-through or rather a snap-back problem. Note that the Riks method again fails to detect the bifurcation point of the defect-free tube SW0. The critical load of 33 aNm can only be found by introducing geometric imperfections, which is not straightforward since the MDFEM elements "know their natural lengths and distances" and thus would relax to the symmetric equilibrium state. In contrast, dynamic time integration schemes such as HHT and Euler backward allow for a direct calculation of the critical load. When introducing Stone-Wales defects, the aforementioned snap-back behavior occurs, i.e., the defects serve as starting points for the failure of the nanotubes. In these cases, the results of the Riks method match their dynamic equivalents.

The critical load drops from 33 aNm without defects to 20-22 aNm with defects.

For the bending tests, all critical loads are detected by the arc-length method. The reason for this is that no material failure, but a pure snap-through problem occurs. The critical loads 24 aNm for SW0 and approx. 22 aNm for SW1, SW2 and SW3 match the ones computed using HHT and Euler backward. The offset in the load-deflection curves for SW1 and SW2 is caused by the non-symmetric Stone-Wales defects which lead to a curvature of the nanotube during the conformational analysis.

6. Conclusions

As a conclusion, the question given in the title of this paper shall be answered. Shell and continuum elements should not be used for molecular dynamic simulations since they are not able to capture the interatomic relations properly. Our examples show that a straightforward application of truss and beam

elements also leads to a number of problems when multi-body potentials are to be considered:

- material parameters for angle bend and torsion cannot be identified uniquely
- there might be false results, especially when loads are applied locally
- there is no distinction between natural and equilibrium bond lengths and angles.

Workarounds are to either use a Tersoff-Brenner type force field which has no bending or torsion potentials or to apply the extended beam technique where all rotational degrees of freedom are eliminated on the element level. For large deformations, we recommend the molecular dynamic finite element method (MDFEM) which is based on special 2-, 3- and 4-noded user elements. MDFEM allows for an efficient modeling and simulation of molecular structures using any finite element software code. It can be applied to large concurrent multiscale analyses, where only parts of a material that are assumed to be important (e.g. interfaces) are modeled using MD elements, while bulk material regions are handled using continuum elements.

Acknowledgement

The authors acknowledge funding by the Helmholtz Association of German Research Centres. The Institute of Structural Analysis (ISD) is member of its virtual institute "Nanotechnology in Polymer Composites". ISD is also member of the Laboratory of Nano and Quantum Engineering (LNQE), the support of which is gratefully acknowledged.

Alder, B., Wainwright, T., 1957. Phase transition for a hard sphere system. Journal of Chemical Physics 27, 1208–1209.

Brenner, D. W., 1990. Empirical potential for hydrocarbons for use in simulating the chemical vapor deposition of diamond films. Physical Review B 42 (15), 9458–9471.

Chen, X., Cao, G., 2006. A structural mechanics study of single-walled carbon nanotubes generalized from atomistic simulation. Nanotechnology 17, 1004–1015.

Chwal, M., 2011. Influence of vacancy defects on the mechanical behavior and properties of carbon nanotubes. Procedia Engineering 10, 1579–1584.

Ding, H., Chen, S. J., Cheng, K., 2007. The atomic-scale finite-element modelling of single-walled carbon nanotubes. Proceedings of the Institution of Mechanical Engineers, Part C: Journal of Mechanical Engineering Science 221, 613–617.

Fan, C. W., Liu, Y. Y., Hwu, C., 2009. Finite element simulation for estimating the mechanical properties of multi-walled carbon nanotubes. Applied Physics A 95, 819–831.

Hu, N., Fukunaga, H., Lu, C., Kameyama, M., Yan, B., 2005. Prediction of elastic properties of carbon nanotube reinforced composites. Proceedings of the Royal Society A 461, 1685–1710.

Hu, N., Nunoya, K., Pan, D., Okabe, T., Fukunaga, H., 2007. Prediction of buckling characteristics of carbon nanotubes. International Journal of Solids and Structures 44, 6535–6550.

Iijima, S., 1991. Helical microtubules of graphitic carbon. Letters To Nature 354 (7), 56–58.

Kalamkarov, A. L., Georgiades, A. V., Rokkam, S. K., Veedu, V. P., Ghasemi-Nejhad, M. N., 2006. Analytical and numerical techniques to predict carbon nanotubes properties. International Journal of Solids and Structures 43, 6832–6854.

Lau, K.-T., Chipara, M., Ling, H.-Y., Hui, D., 2004. On the effective elastic moduli of carbon nanotubes for nanocomposite structures. Composites Part B: Engineering 35, 95–101.

Leung, A. Y. T., Guo, X., He, X. Q., Kitipornchai, S., 2005. A continuum model for zigzag single-walled carbon nanotubes. Applied Physics Letters 86, 083110.

Li, C., Chou, T.-W., 2003a. Elastic moduli of multi-walled carbon nanotubes and the effect of van der Waals forces. Composites Science and Technology 63, 1517–1524.

Li, C., Chou, T.-W., 2004. Modeling of elastic buckling of carbon nanotubes by molecular structural mechanics approach. Mechanics of Materials 36 (11), 1047–1055.

Li, C. Y., Chou, T. W., 2003b. A structural mechanics approach for the analysis of carbon nanotubes. International Journal of Solids and Structures 40, 2487–2499.

Liu, B., Huang, Y., Jiang, H., Qu, S., Hwang, K. C., 2004. The atomic-scale finite element method. Computer Methods in Applied Mechanics and Engineering 193, 1849–1864.

Mayo, S. L., Olafson, B. D., Goddard (III), W. A., 1990. DREIDING: A generic force field for molecular simulations. Journal of Physical Chemistry 94, 8897–8909.

Meo, M., Rossi, M., 2006. Prediction of Young's modulus of single wall carbon nanotubes by molecular-mechanics based finite element modelling. Composites Science and Technology 66, 1597–1605.

Miller, R. E., Tadmor, E. B., 2009. A unified framework and performance benchmark of fourteen multiscale atomistic/continuum coupling methods. Modelling and Simulation in Materials Science and Engineering 17 (5), 053001.

Nahas, M. N., Abd-Rabou, M., 2010. Finite element modeling of carbon nanotubes. International Journal of Mechanical & Mechatronics Engineering 10, 19–24.

Nasdala, L., Kempe, A., Rolfes, R., 2010. The Molecular Dynamic Finite Element Method (MDFEM). Computers, Materials & Continua 19 (1), 57–104.

Odegard, G. M., Gates, T. S., Nicholson, L. M., Wise, K. E., 2002. Equivalent-continuum modeling of nano-structured materials. Composites Science and Technology 62, 1869–1880.

Parvaneh, V., Shariati, M., Sabeti, A. M. M., 2009. Investigation of vacancy defects effects on the buckling behavior of SWCNTs via a structural mechanics approach. European Journal of Mechanics - A/Solids 28, 1072–1078.

Rahman, A., 1964. Correlations in the motion of atoms in liquid argon. Physical Review A 136, 405–411.

Rossi, M., Meo, M., 2009. On the estimation of mechanical properties of single-walled carbon nanotubes by using a molecular-mechanics based FE approach. Composites Science and Technology 69, 1394–1398.

Saavedra Flores, E. I., Adhikari, S., Friswell, M. I., Scarpa, F., 2011. Hyperelastic finite element model for single wall carbon nanotubes in tension. Computational Materials Science 50 (3), 1083–1087.

Sakhaee-Pour, A., Ahmadian, M. T., 2007. Finite element model of SWCNT under hydrostatic pressure. AIP Conference Proceedings 929, 82–88.

Shokrieh, M. M., Rafiee, R., 2010. Prediction of young's modulus of graphene sheets and carbon nanotubes using nanoscale continuum mechanics approach. Materials and Design 31, 790–795.

Theodosiou, T. C., Saravanos, D. A., 2007. Molecular mechanics based finite element for carbon nanotube modeling. Computer Modeling in Engineering & Sciences 19, 121–134.

Theodosiou, T. C., Saravanos, D. A., 2011. Numerical simulations using a molecular mechanics-based finite element approach: Application on Boron-Nitride armchair nanotubes. International Journal for Computational Methods in Engineering Science and Mechanics 12, 203–211.

Tserpes, K. I., Papanikos, P., 2005. Finite element modeling of single-walled carbon nanotubes. Composites Part B: Engineering 36, 468–477.

Wackerfuß, J., 2009. Molecular mechanics in the context of the finite element method. International Journal for Numerical Methods in Engineering 77, 969–997.

Wang, Q., 2004. Effective in-plane stiffness and bending rigidity of armchair and zigzag carbon nanotubes. International Journal of Solids and Structures 41, 5451–5461.

Wang, X. Y., Wang, X., 2004. Numerical simulation for bending modulus of carbon and some explanations for experiment. Composites Part B: Engineering 35, 79–86.

Wang, Y., Sun, C., Sun, X., Hinkley, J., Odegard, G. M., Gates, T. S., 2003. 2-D nano-scale finite element analysis of a polymer field. Composites Science and Technology 63, 1581–1590.

Yoon, J., Ru, C. Q., Mioduchowski, A., 2004. Timoshenko-beam effects on transverse wave propagation in carbon nanotubes. Composites Part B: Engineering 35, 87–93.

Zhang, H. W., Yao, Z., Wang, J. B., Zhong, W. X., 2007. Phonon dispersion analysis of carbon nanotubes based on inter-belt model and symplectic solution method. International Journal of Solids and Structures 44, 6428–6449.

Zhu, S. Q., Wang, X., 2007. Effect of environmental temperatures on elastic properties of single-walled carbon nanotube. Journal of Thermal Stresses 30, 1195–1210.